# Suppression of ionic doping by molecular dopants in conjugated polymers for improving specificity and sensitivity in biosensing applications

Hyun-June Jang<sup>†</sup>, Yunjia Song, Justine Wagner, Howard E. Katz\*

Department of Materials Science and Engineering, Johns Hopkins University, 3400 N. Charles St, Baltimore, MD 21218-2608, USA

KEYWORDS: P3HT, PT-COOH, Ionic doping, F4TCNQ doping, Sequential doping, RGFET, OECT

ABSTRACT: Ionic doping effects in conjugated polymers often cause non-specific signaling and a low selectivity of bioelectronic sensing. Using remote-gate field-effect transistor characterization of molecular and ionic doping in poly(3-hexylthiophene) (P3HT) and acid-functionalized polythiophene, poly [3-(3-carboxypropyl) thiophene-2,5-diyl] (PT-COOH), we discovered that proton doping effects on the interfacial potential occurring in P3HT could be suppressed by sequentially doping P3HT by 2,3,5,6-tetrafluoro-7,7,8,8-tetracyanoquinodimethane (F4TCNQ). To be specific, intrinsic pH sensitivity shown by pure P3HT (18 mV/pH in a range from pH 3 to 9) was fully dissipated for doped P3HT:F4TCNQ. However, F4TCNQ sequential doping instead increases pH sensitivity of acid-functionalized polythiophene, PT-COOH (40 mV/pH), compared to that of a pure PT-COOH (30 mV/pH). Interactions between polythiophene backbone and side chains, which constrain the activity of COOH, are weakened by stronger F4TCNQ doping leaving behind responsive COOH groups exposed to aqueous solutions. This is supported by the reduced pH sensitivity of PT-COOH sequentially doped by a weaker dopant, tetracyanoethylene (TCNE) (21 mV/pH). Thus, doping is shown to stabilize a nonpolar conjugated polymer to pH-induced fluctuations on one hand, and to activate a COOH side chain to pH-induced response on the other.

## Introduction

Field-effect transistor (FET) biosensors have drawn huge attention over the past decades because of their rapid, label-free detection, and high sensitivity to targeted molecules. The multiple laboratory processes for conventional immunoassays such as enzyme-linked immunosorbent assay (ELISA)- or polymerase chain reaction (PCR)- based detections could be reduced in number using a label-free FET sensing format as part of a "lab-on-a-chip" system. These FET bioelectronic platforms are potentially useful for point-of-care testing that enables on-spot diagnostics of widespread and contagious infections.

While intrinsic electrochemical, physical, and mechanical properties of semiconducting and sensing materials determine characteristic of the detection platform, conducting polymers (CPs) based on polyaniline, polypyrrole, and polythiophene (PT) have gained significant attention with increasing needs for wearable electronics. <sup>5-8</sup> CPs offer lowcost production, stretchability, enhanced stability, long lifetime, and fast response in ionic liquids. <sup>9</sup>

One of the most promising and widely used CPs is poly(3,4-ethylenedioxythiophene):poly(styrenesulfonate) (PEDOT:PSS).<sup>10</sup> Conducting conjugated PEDOT with positive charges interacts with insulating PSS with negative charges via strong Columbic attractions. PEDOT is insoluble in water, but insulating PSS facilitates the dispersion of PEDOT in water. Mobile holes in the PEDOT backbones are

compensated by sulfonate acceptors on the PSS. Thus, PEDOT:PSS-based organic electrochemical transistors (OECTs) has been regarded as one of the most promising FET sensing platforms for wearable bioelectronics thanks to the mixed electron/hole and ion transport in the aqueous environment.<sup>11</sup> That is, conductivity of CPs is strongly modulated by transfer of doping/de-doping ions between a solution and the entire volume of CPs.<sup>12</sup>

Nonetheless, it is often challenging to modify PEDOT:PSS via synthesis, 13 such as to incorporate carboxylic or amino acid groups that are useful for functionalization by biorecognition elements such as antibodies, enzymes, and DNA. Therefore, PEDOT:PSS is often blended with functionalized additives. A finely balanced PEDOT:PSS solution, however, could be disturbed by additions of extraneous additives or solvents, causing disruption of conductivity of PEDOT:PSS films and having significant impact on the electrical performance of PEDOT:PSS. 14 Alternatively, biological moieties are functionalized on a gate electrode of OECT devices 15-16 or over electrolytes 17 instead of at interfaces between the PEDOT:PSS and electrolyte.

Also, CPs also hold drawbacks regarding their selectivity as biosensing interfacial materials<sup>6</sup> because any solute able to undergo oxidation or reduction at CPs provokes electrical fluctuations regardless of whether it was the targeted analyte. However, complicated polymorphic aspects of CPs including crystalline and amorphous domains complicate our

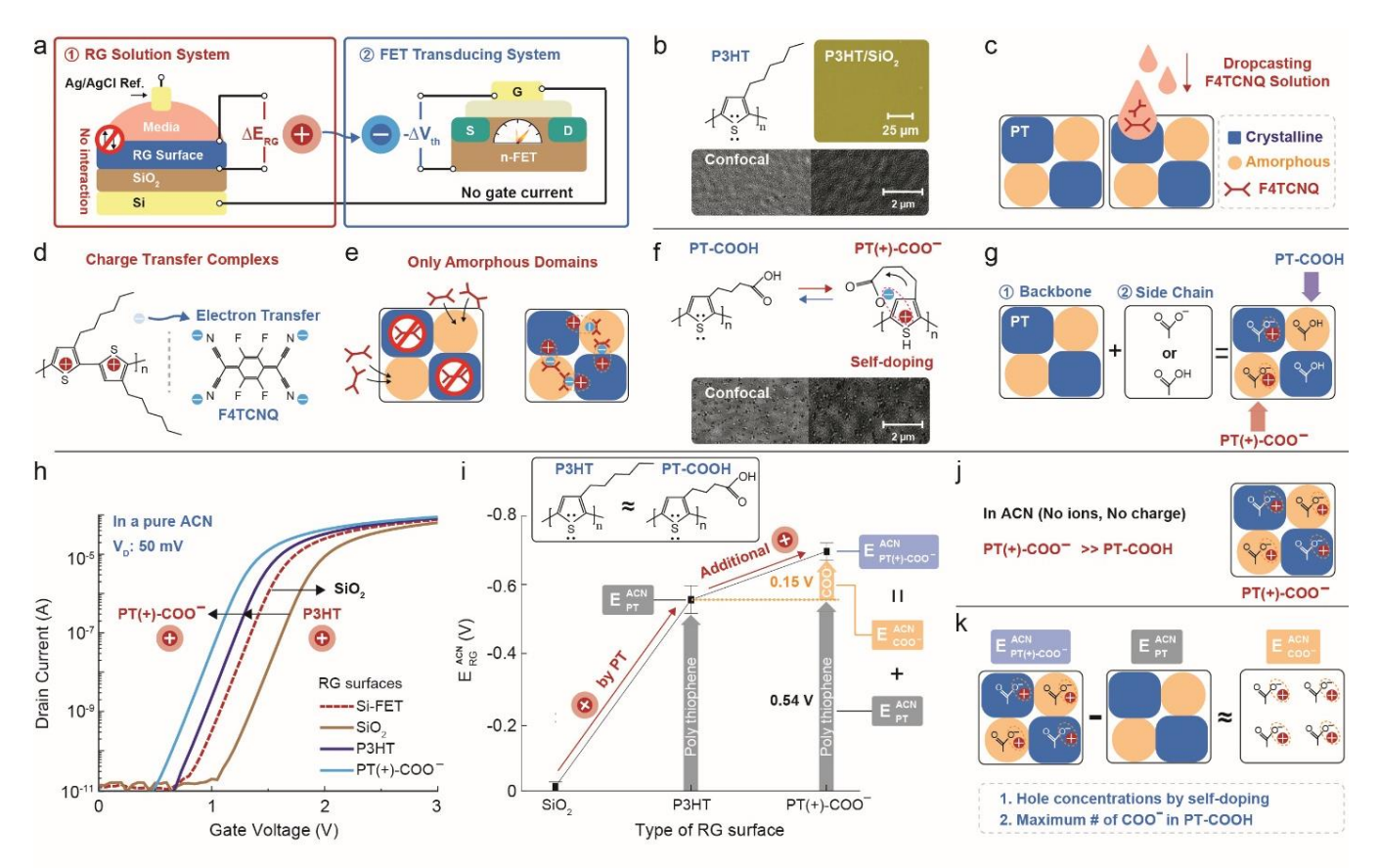


**Figure 1.** Schematic images of the RGFET system combining RG solution system and FET transducing system. (b) Chemical structure of P3HT and microscopic images of P3HT on SiO<sub>2</sub> surface. Confocal microscopic images of the same P3HT films with different contrasts are shown below. (c) Schematic diagram of the P3HT film including amorphous and crystalline domain and sequential solution doping method. (d) Chemical structure of charge transfer complexes between P3HT and F4TCNQ. (e) Schematic diagram of the F4TCNQ doping in P3HT. (f) Chemical structure of PT-COOH and confocal microscopic images of PT-COOH on SiO<sub>2</sub> surface with different contrasts. (g) Schematic diagram of the polymorphic systems of PT-COOH. (h) Representative transfer curves of the RGFETs with the RG of SiO<sub>2</sub>, P3HT/SiO<sub>2</sub>, and PT-COOH/SiO<sub>2</sub> measured in ACN. Transfer curve of intrinsic Si-FET without a connection of the RG is compared in the same plot. (i)  $E_{RG}^{ACN}$  distributions at least over 8 samples as a function of the type of RG surfaces. (j) Schematic diagram of PT(+)-COO<sup>-</sup> in ACN. (k) Schematic diagram for  $E_{COO}^{ACN}$ 

understanding of ionic doping effects in CPs. <sup>18</sup> With a variety of options for tailoring specific properties of CPs, progress in bioelectronics requires better understanding of origins of ionic doping effects to address issues mentioned above.

Herein, we first aim to investigate factors that control ionic doping in a PT backbone by using remote-gate field-effect transistor (RGFET) characterization and then propose a way to suppress undesirable ionic doping by using sequential chemical doping methods. <sup>19</sup> We discover that intrinsic pH sensitivity shown by regioregular poly(3-hexylthiophene) (P3HT) is completely dissipated on P3HT films sequentially doped by 2,3,5,6-tetrafluoro-7,7,8,8-tetracyanoquinodimethane (F4TCNQ). It is interpreted that F4TCNQ has already oxidized all dopable sites in amorphous domains in P3HT, deactivating the films for proton doping and leaving no other significant mechanism for proton interaction with P3HT.

The result suggests a facile way to achieve highly stable PT-based CPs that could even incorporate receptor-functionalizable carboxylic acid groups, such as starting from regioregular poly [3-(3-carboxypropyl) thiophene-2,5-diyl

(PT-COOH). Such functionality is much more difficult to incorporate into PEDOT:PSS. However, PT-COOH itself is complicated by additional interactions between PT backbones and COOH side chains that lead to self-doping.  $^{20-22}$  Hole carriers are injected into the main backbone of the  $\pi$ -conjugated system that is compensated by proton reduction or transfer occurring at/from the acidic COOH moiety, resulting in the formation of a carboxylate moiety that serves as the oppositely charged counterion. We investigated this critical role of COOH groups in PT-COOH by comparing it with P3HT.

Finally, we discover self-doping in PT-COOH is mitigated by F4TCNQ doping while pH response by COOH groups in PT-COOH is enhanced. Electrons from the polymer main chains appear to be drawn to the strong electron acceptor F4TCNQ rather than to the acidic protons, which results in decreased interactions between PT and COOH leaving behind active COOH groups that are free to respond to protons. This is supported by the observed decreased pH sensitivity of PT-COOH sequentially doped by the weaker electron acceptor tetracyanoethylene (TCNE), which does not compete as effectively for electrons.

#### **Results and Discussion**

**RGFET setup and definition.** The RGFET structure isolates a sensing surface from the FET transducer (Figure 1a). An RG solution system consists of an Ag/AgCl reference electrode, a media solution, and an RG material. The RG surface, here P3HT or PT-COOH, is electrically coupled to the gate of a Si-FET via a Si electrode underneath  $\text{SiO}_2$ . Increased positive electric potentials in the RG system lead to the same amount of reduction in  $V_{th}$  of the RGFET by making the n-FET transducer turn on more easily.

Current flow over the conjugated polymers is completely blocked in this configuration, as shown in Figure S1. Moreover, the input impedance of a Si-FET chip is at least 100 times higher than those of our typical RG module (Figure S2). Therefore,  $V_{th}$  of the RGFET is an independent variable from factors that could alter the impedance of RG modules such as the thickness of the RG materials and  $SiO_2$  and the contact area of media on the RG surface, as shown in our previous work. That is, the RGFET only translates electrochemical potentials at the solution interface to the gate of the Si-FET.

A P3HT film is spin-coated on the SiO<sub>2</sub> substrate as the RG surface, shown to be essentially continuous (Figure 1b, optical image in Figure S3a). Extensive literature has already reported that P3HT films have semi-crystalline microstructures consisting of crystalline P3HT separated by amorphous domains, 19, 24-27 schematically shown as a simplified diagram in Figure 1c). Highly conductive P3HT films could be obtained by the sequential doping method of drop-casting an F4TCNQ-ACN solution on the pure P3HT film. F4TCNQ doping is facilitated by electron transfer from the HOMO level of the host P3HT to the LUMO of the F4TCNQ molecule, leaving behind polarons or bipolarons on PT backbones of P3HT (Figure 1d).

P3HT is completely insoluble and appears non-swellable in the ACN solution. This means that there is little or no changed conformation of P3HT during the sequential doping process. It is well known for sequential doping that F4TCNQ anions are preferentially infiltrated in P3HT amorphous domains up to a 4.9 mol% solubility limit. 19,24-26 Thus, sequentially doped P3HT films reveal almost identical surface roughness to that of pristine P3HT film. 19,25 Holes generated by the doping reaction preferentially move to the crystalline regions due to their higher HOMO levels 28-29 as depicted in Figure 1e.

The chemical structure of regionegular PT-COOH is similar to that of P3HT except for their carboxylic acid groups in side chains. Crystallites of PT-COOH are seen in microscopic images in Figure 1f (confocal) and Figure S3b (optical). PT-COOH shows self-doping effects from carboxylic acid groups.<sup>20-22</sup> The negatively charged carboxylate stabilizes positive charges on the backbone by electrostatic interactions (Figure 1f), enabling higher hole carrier concentrations on the polymer backbone.<sup>22</sup> The self-doping effects in PT-COOH are supported by our prior studies<sup>23, 30</sup> of a large intrinsic hole concentration ( $p_0$ ) of 1.06 x  $10^{19}$  /cm<sup>3</sup> for PT-COOH, compared to that of P3HT film  $(2.4 \times 10^{17} / \text{cm}^3)$ . This result also corresponds to a higher drain current in the OFET device structure with PT-COOH (~ mA) as semiconductor than with P3HT ( $\sim \mu A$ ) (Figure S4). It should be understood that the polymer we refer to as "PT-COOH" can

exist as a mixture of multiple forms, for example, the neutral thiophene polymeric main chain with COOH side chains, the doped form with a positively charged main chain, COOH side chains, and extrinsic counterions, the self-doped form with positive charges on the main chain and COO- counterion side chains, and a side-chain ionized form with a neutral main chain and COO- side chains. Mixtures and hybrids of these are also possible.

We model a polymeric system of PT-COOH consisting of two individual functional components: 1) PT and 2) COOH or COO-, based on the assumptions of additional effects coming from side chains in PT backbones (Figure 1g). Side chains vary from COOH to COO- depending on the environments. We also presume PT backbones in PT-COOH play the same role as in P3HT. PT(+)-COO- infers self-doping effects and higher hole concentration in PT backbones than P3HT and PT-COOH. PT(+)-COO- is more energetically favorable in contact with the non-reactive but polarizable ACN solution (no charge, no ions in ACN). In contrast, PT-COOH could be more preferred in water at more acidic pH, as COOH groups equilibrate with protons in aqueous solutions that also supply counterions.

Figure 1h shows representative transfer curves of the Si-FET itself and the RGFETs with the RG of SiO<sub>2</sub>, P3HT, and PT(+)-COO<sup>-</sup> measured in a pure non-polar ACN solution. There are no changes in the other electrical parameters such as subthreshold swing and transconductance (Figures 1h and S5) over all transfer curves except for changes in V<sub>th</sub> by the series electrical potential imposed on the RG system. V<sub>th</sub> is 1.8, 1.26, and 1.13 V on average from the RGs of SiO<sub>2</sub>, P3HT, and PT(+)-COO<sup>-</sup>, respectively. Lower V<sub>th</sub> in PT(+)-COO<sup>-</sup> than P3HT (Figure 1h) supports that PT(+)-COO<sup>-</sup> is dominant over the PT-COOH fraction in contact with the ACN solution assuming that the electrical potential of P3HT is almost identical to that of PT-COOH (Inset of Figure 1i).

In classic semiconductor physics $^{31}$ ,  $V_{th}$  of the RGFET is a sum of electric potentials of each component in the RGFET:

$$V_{\rm th} = V_{\rm FET} + E_{\rm ref} + \phi_{lj} - \varphi_s + \chi_{sol} + \frac{\phi_{RG}}{q}$$
 (1)

where  $V_{FET}$  is  $V_{th}$  of a Si-FET,  $E_{ref}$  is absolute potential of the reference electrode,  $\phi_{lj}$  is the liquid junction potential difference,  $\varphi_s$  is the surface potential at the electrolyte/sensing film interface,  $\chi_{sol}$  is the electrolyte insulator surface dipole potential, and  $\phi_{RG}$  is work function (in energy units) of the RG material.  $V_{FET}$  (1.5 V) and  $E_{ref}$  (0.316 V) are consistent over our all experiments.  $\Delta V_{th}$  from that of the Si-FET originates from intrinsic electric potentials of RG materials as an ACN medium mostly acts as a solution dielectric without interaction with RG materials. We further define standard electric potential ( $E_{RO}^{RO}$ ) within equation (1) which is only associated with properties of intrinsic electric potentials of overlying solution, RG material and its contact.

$$E_{RG}^{Sol} = \phi_{lj} - \varphi_s + \chi_{sol} + \frac{\phi_{RG}}{q} \quad (2)$$

where the superscript of  $E_{RG}^{Sol}$  is the type of solution placed on the RG surface such as ACN, F4TCNQ, and pH (F4TCNQ:

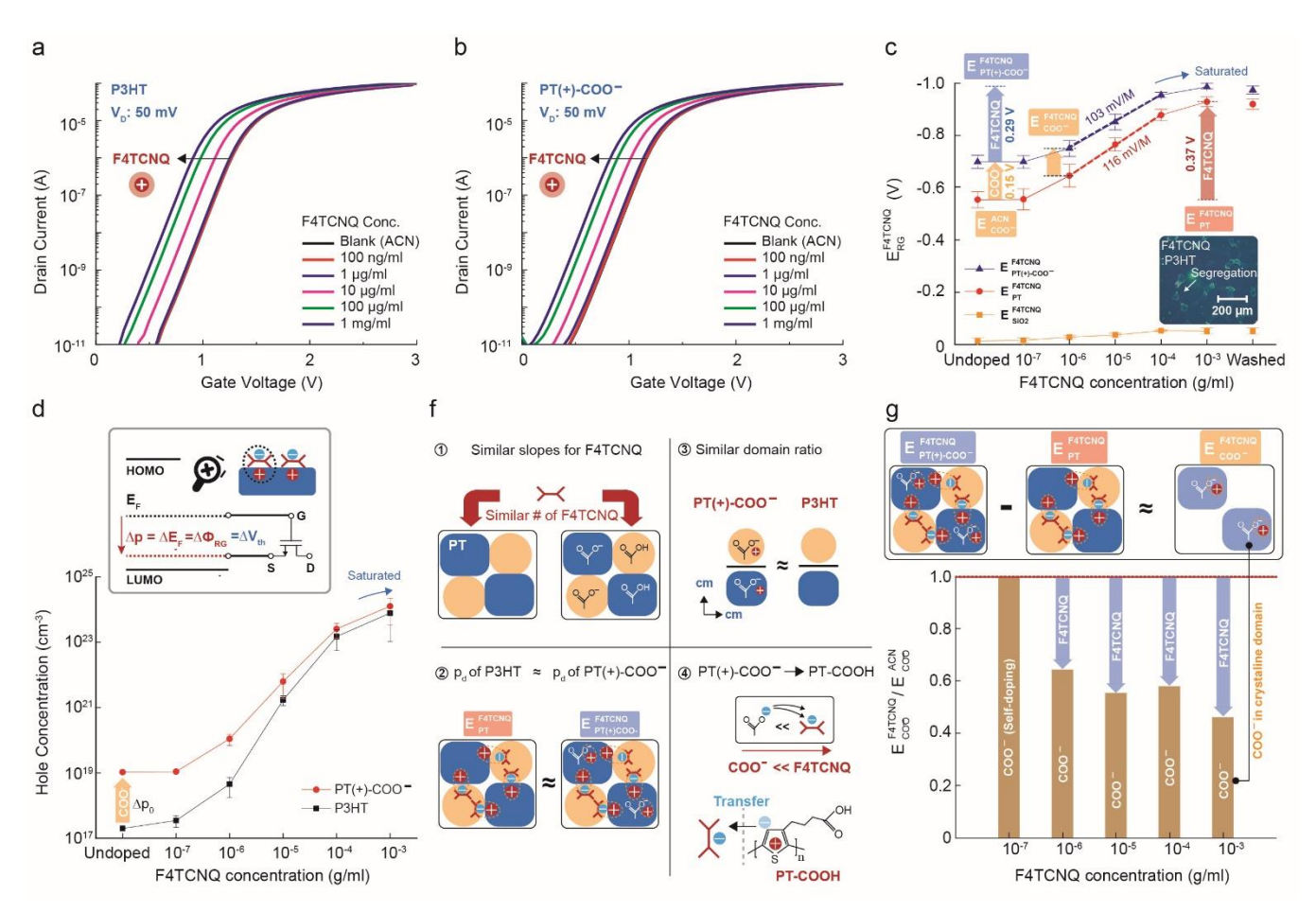


**Figure 2.** Representative transfer curves of the RGFETs with the RG of (a) P3HT/SiO<sub>2</sub> and (b) PT(+)-COO<sup>-</sup>/SiO<sub>2</sub> with increasing concentrations of F4TCNQ. (c)  $E_{RG}^{F4TCNQ}$  values over at least 8 samples as a function of F4TCNQ concentrations. Inset shows microscopic images of P3HT films doped by 1 mg/ml F4TCNQ. (d) Hole concentrations of P3HT and PT(+)-COO<sup>-</sup> as a function of increasing F4TCNQ concentrations. Inset shows energy band diagrams of P3HT resulting from F4TCNQ doping where  $E_F$ , and  $\Phi_{RG}$  are Fermi level and work function of RG materials and the resultant  $\Delta V_{th}$  translated by the Si-FET. (f) Schematics of detailed mechanisms of F4TCNQ doping in P3HT and PT(+)-COO<sup>-</sup> films. (g)  $E_{COO^-}^{F4TCNQ}/E_{RG}^{ACN}$  as a function of F4TCNQ concentrations. Inset shows schematic diagram for  $E_{COO^-}^{F4TCNQ}$ .

F4TCNQ solution dissolved in ACN, pH: aqueous solution at a given pH). The subscript of  $E_{RG}^{Sol}$  is the type of RG surface.

 $E_{RG}^{Sol}$  of SiO<sub>2</sub> in ACN ( $E_{SiO2}^{ACN}$ ) should be set to 0 V meaning that the SiO<sub>2</sub>-ACN interface should not be ionically polarized.  $E_{RG}^{Sol}$  of P3HT in ACN ( $E_{PT}^{ACN}$ ) significantly decreases by 0.54 V resulting from initial hole concentrations in PT backbones of P3HT with counterions closer to the solvent surface. Further decrease of  $E_{RG}^{Sol}$  of PT(+)-COO- ( $E_{PT(+)COO-}^{ACN}$ ) relative to that of P3HT is caused by additional hole concentration resulting from interactions between side chains and PT backbones. We approximately estimate the electrical potential originating from hole concentration compensated by self-doping effects (side chain effects) by subtracting  $E_{PT}^{ACN}$ of P3HT from  $E_{PT(+)COO-}^{ACN}$  of PT-COOH; we designate that value as  $E_{COO}^{ACN}$ . The COO- counterions seem to be directed more toward the solvent.  $E_{COO}^{ACN}$  is schematically described in Figure 1k. In our experiment setup, the fraction of COOin a PT-COOH film would be maximized in a non-reactive ACN solution while COO- side chains interact with PT backbones via Columbic attractions.

Molecular doping effect. We now turn our attention to sequential F4TCNQ doping effects in P3HT and PT(+)-COOfilms. Sequential doping method results in smooth morphology of doped PT-COOH films (Figure S6) as was case for F4TCNQ:P3HT films in our previous work.<sup>23</sup> Again,  $E_{RG}^{F4TCNQ}$ refers to electrical potential of a specific RG surface such as SiO<sub>2</sub>, P3HT, and PT(+)-COO- in contact with an F4TCNQ solution dissolved in ACN. A pure SiO<sub>2</sub> surface presents hardly any response to the increased F4TCNQ concentrations ranging from 100 ng/mL to 1 mg/mL (Figure S7) because little or no interaction occurs between F4TCNQ and SiO<sub>2</sub>. In contrast, F4TCNQ promotes similar shifts of transfer curves from the RGs of P3HT (Figure 2a) and PT(+)-C00  $^{\circ}$  (Figure 2b). In particular, lower  $E_{RG}^{F4TCNQ}$  shown over P3HT and PT(+)-COO- (Figure 2c) indicates additional positive potentials applied on the P3HT and PT(+)-C00- surfaces from F4TCNQ doping. Each  $E_{RG}^{F4TCNQ}$  is calculated from the last value of each V<sub>th</sub> for 20 consecutive measurements in a specific F4TCNQ concentration (Figure 8). Both  $E_{PT}^{F4TCNQ}$  and  $E_{PT(+)COO_{-}}^{F4TCNQ}$  saturate upon 1 mg/ml F4TCNQ solution where F4TCNQ molecules begin to aggregate on each surface due

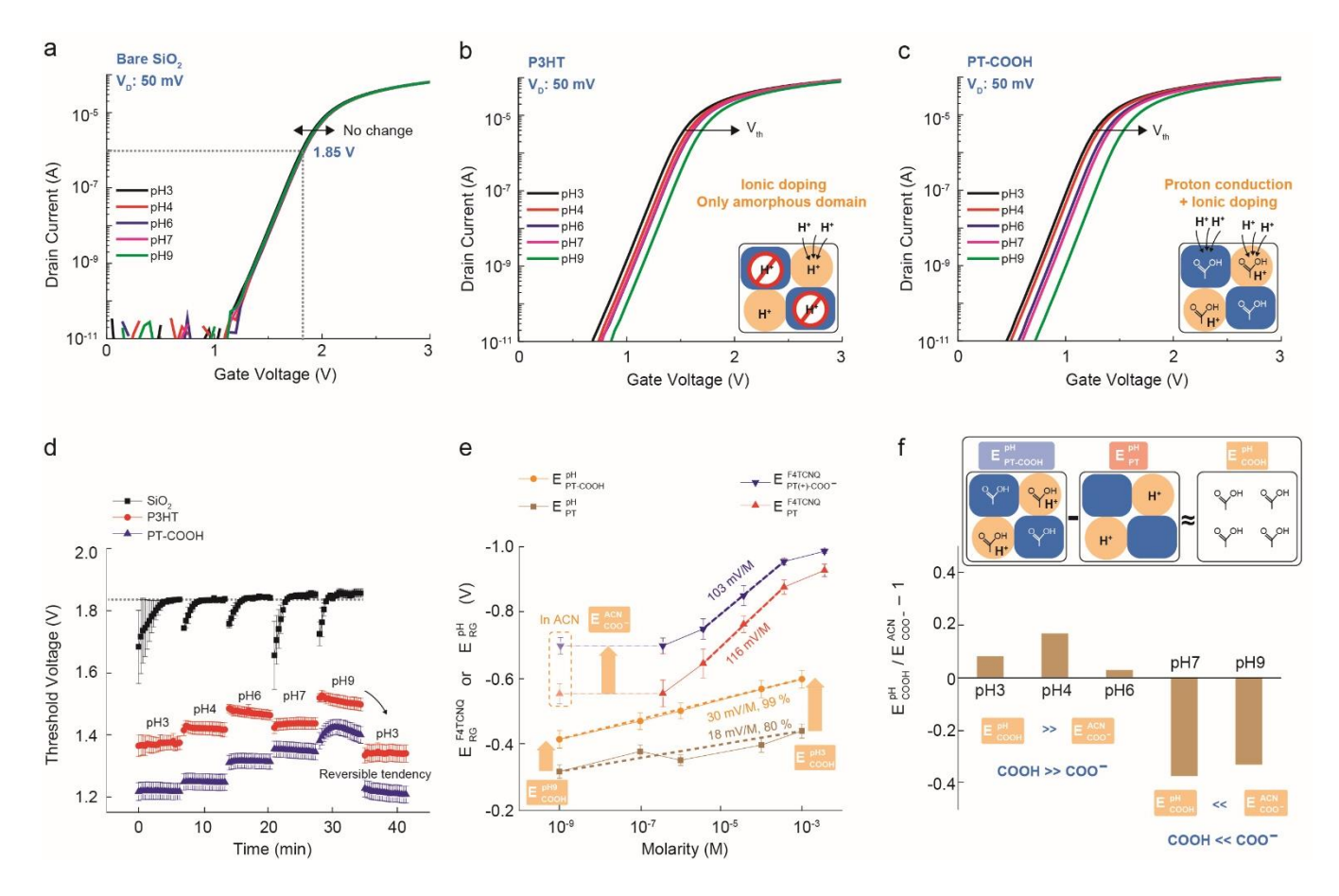


**Figure 3.** Representative transfer curves of the RGFETs with the RG of (a) SiO<sub>2</sub>, (b) P3HT/SiO<sub>2</sub> and (c) PT-COOH/SiO<sub>2</sub> depending on pH values in a range from 3 to 9. (d)  $V_{th}$  distributions of SiO<sub>2</sub>, P3HT, and PT-COOH at least over 8 samples in terms of increasing pH values over time. (e)  $E_{RG}^{F4TCNQ}$  or  $E_{RG}^{pH}$  as a function of concentrations of proton and F4TCNQ. (f) Comparison between  $E_{COOH}^{pH}$  and  $E_{COO-}^{ACN}$  vs pH values. Inset shows schematic diagram for  $E_{COOH}^{pH}$ .

to their solubility limits of F4TCNQ in PT backbones (Inset of Figure 2c). The saturated  $E_{PT}^{F4TCNQ}$  and  $E_{PT}^{F4TCNQ}$  is mostly maintained even after aggressive washing of the surfaces 3 times with pure ACN, implying that the doping effect is mostly irreversible. For a linear responsive regime in a range from 1 to 100 µg/ml F4TCNQ, slopes of  $E_{RG}^{F4TCNQ}$  are calculated to be 103 and 116 mV/M for PT(+)-COO- and P3HT, respectively. Maximum absolute values of  $\Delta E_{PT}^{F4TCNQ}$  and  $\Delta E_{PT}^{F4TCNQ}$  from each  $E_{PT}^{ACN}$  and  $E_{PT}^{ACN}$  are 0.37 V and 0.29 V, respectively (i.e. before/after doping at 1 mg/ml F4TCNQ).

In our previous work<sup>23</sup>, we connected  $\Delta V_{th}$ , or  $\Delta E_{RG}^{F4TCNQ}$ , to the change in work functions as polymer is doped (Inset of Figure 2d). By assuming no loss in hole concentrations from any electron transfer or interface traps between SiO<sub>2</sub> and CPs, we have the following equation to express the hole concentrations of doped films (p<sub>d</sub>):

$$p_{d} = p_{0} \exp\left(-\frac{\Delta E_{RG}^{F4TCNQ}}{kT}\right) (3)$$

where k is the Boltzmann constant, and T is temperature (K). Based on  $p_0$  of P3HT (2.4 ×  $10^{17}$  /cm³) and PT(+)-COO-(1.06 x  $10^{19}$  /cm³) aforementioned,  $p_d$  of each polymer is

calculated in Figure 2d. The actual value of  $\Delta E_{RG}^{F4TCNQ}$  is negative as  $\Delta E_{RG}^{F4TCNQ}=E_{RG}^{ACN}-E_{RG}^{F4TCNQ}$  and thus  $p_d$  increases as a polymer is doped. Interestingly, a large difference in intrinsic hole concentrations ( $\Delta p_0$ ) between P3HT and PT(+)-C00 $^-$  is highly decreased for the heavily doped films that show mostly identical  $p_d$  (Figure 2d). It is noted that  $\Delta p_0$  stems from self-doping effects of PT(+)-C00 $^-$  in our assumption.

Our observations so far bring up several conclusions shown schematically in Figure 2f. First, similar slopes of  $E_{PT}^{F4TCNQ}$  and  $E_{PT(+)COO-}^{F4TCNQ}$  in Figure 2c indicates similar F4TCNQ doping reactions for both polymers. It is interpreted that only the backbone is engaged in F4TCNQ doping reactions. It is noted that variations in electrochemical potentials of P3HT and PT(+)-COO- for every 10-fold increase in F4TCNQ concentration are much higher than the Nernst limit of 60 mV/M. This infers strong chemical reactions and electrostatic attractions between F4TCNQ and conjugated polymers beyond simple 1:1 complexation. Second, mostly identical  $p_d$  levels upon solubility limits of F4TCNQ in Figure 2d show that hole concentrations generated by F4TCNQ doping are limited at a similar level. This also infers that

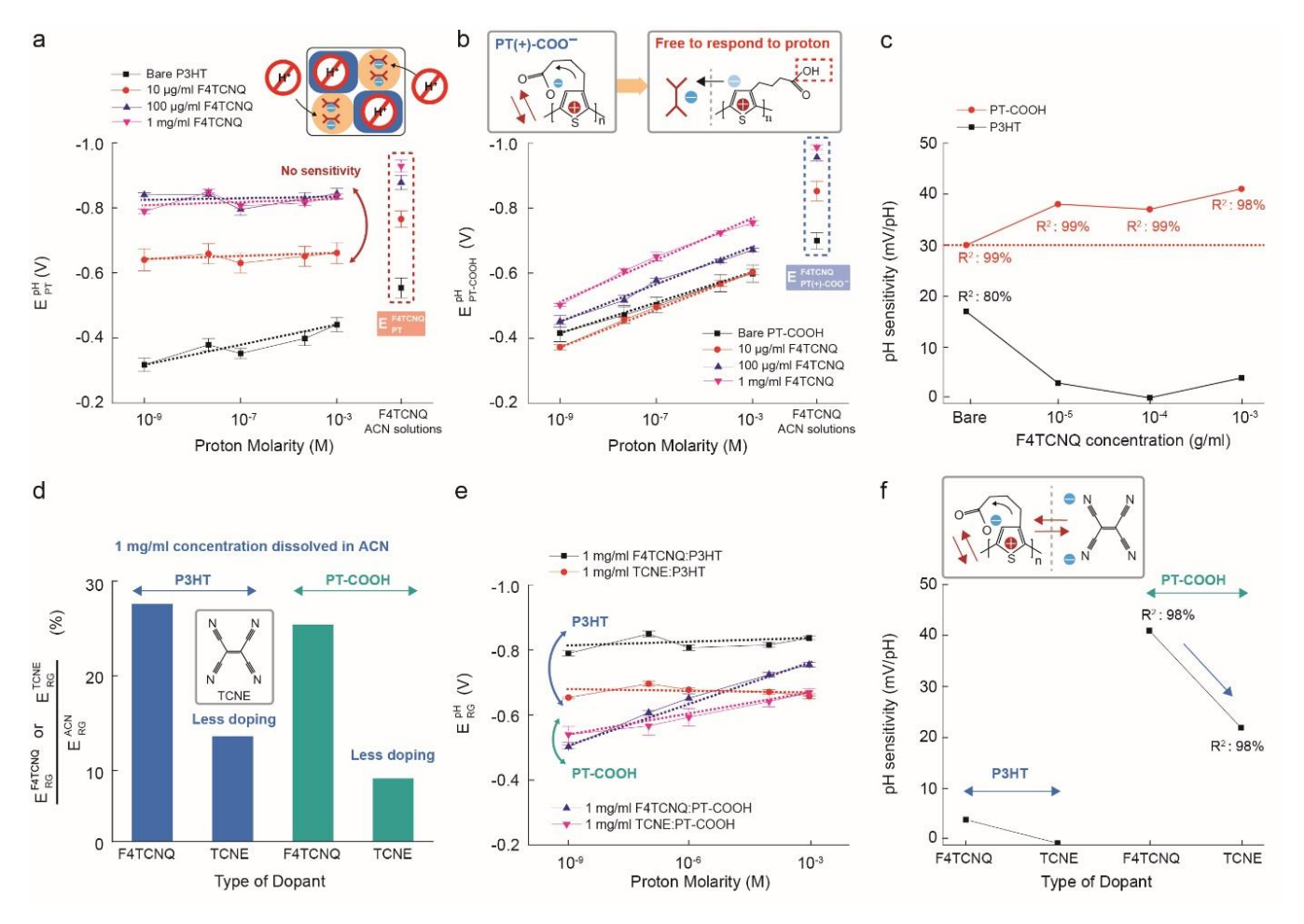


**Figure 4.** (a)  $E_{PT}^{pH}$  distributions of the doped P3HT at least over 8 samples vs proton concentrations. Inset shows schematic diagram of ionic doping in P3HT film. (b)  $E_{PT\cdot COOH}^{pH}$  distributions of the doped PT-COOH at least over 8 samples vs proton concentrations. Inset describes mechanism in the improved pH sensitivity from doped PT-COOH films. (c) pH sensitivity of P3HT and PT-COOH vs F4TCNQ doping concentrations on both polymers. (d)  $E_{PT}^{F4TCNQ}$  variation relative to  $E_{PT}^{ACN}$  and  $E_{PT}^{TCNE}$  and  $E_{PT}^{TCNE}$  and  $E_{PT}^{TCNE}$  and  $E_{PT}^{TCNE}$  distributions of F4TCNQ:P3HT, TCNE:P3HT, F4TCNQ:PT-COOH at least over 6 samples vs proton concentrations on each film. (f) pH sensitivity of F4TCNQ:P3HT, TCNE:P3HT, F4TCNQ:PT-COOH, and TCNE:PT-COOH films.

both polymers could have a similar amorphous/crystalline domain ratio because sequential F4TCNQ doping is only favored in amorphous domains. Finally, self-doping in PT(+)-C00 $^{\rm -}$  is directly replaced with F4TCNQ doping reactions. As a result, a larger fraction of protonated COOH are formed in the PT-C00H:F4TCNQ system as will be further discussed later.

We also calculate a difference in electrical potential between  $E_{PT(+)COO-}^{F4TCNQ}$  and  $E_{PT}^{F4TCNQ}$  which is defined as  $E_{COO-}^{F4TCNQ}$  and schematically illustrated in the inset of Figure 2g.  $E_{COO-}^{F4TCNQ}$  at each F4TCNQ solution concentration ranging from 100 ng/ml to 1 mg/ml is represented as its fractional contribution from F4TCNQ doping (that replaces some self-doping) and the remaining contribution of  $E_{COO-}^{ACN}$  (self-doping) in Figure 2g. Again,  $E_{COO-}^{ACN}$  is a difference in electrical potentials between P3HT and PT(+)-COO- in a pure ACN solution derived from side chain effects.  $E_{COO-}^{F4TCNQ}$  at 100 ng/ml F4TCNQ is identical to  $E_{COO-}^{ACN}$  (shown as contributing all of the threshold voltage or work function shift from doping) because self-doping in PT(+)-COO- is fully maintained for

such a lightly-doped condition. However,  $E_{COO-}^{F4TCNQ}$  is steadily decreased, but not eliminated, with increased F4TCNQ doping, indicating electrons on F4TCNQ instead of carboxylate anions. In particular,  $E_{COO-}^{F4TCNQ}$  at 1 mg/ml F4TCNQ is associated with the number of COO- in crystalline domains of PT-COOH films, where F4TCNQ does not penetrate, while F4TCNQ is only infiltrated in amorphous domains of PT-COOH where it induces a net increase in work function.

**Ionic doping effects in pure polymers.** Figure 3a, 3b, and 3c shows representative responses of transfer curves from  $SiO_2$ , P3HT, and PT-COOH for pH values in a range from 3 to 9.  $E_{RG}^{pH}$  refers to electrical potential of a specific RG surface in contact with aqueous solutions of stated pH. We assumed that PT-COOH could be more preferred than PT(+)-COO- in aqueous solutions. A 300-nm-thick  $SiO_2$  has a limited pH sensitivity (3 mV/pH with the linearity of 87%) due to a hydrated  $SiO_2$  surface (Figure S9). P3HT deposited on  $SiO_2$ , however, shows responses to different proton concentrations (Figure 2b) which could not be explained by a site-binding model.<sup>32</sup> Instead, this response is from ionic

doping effects in  $\pi$ -conjugated polymers such as P3HT.<sup>18, 33</sup> Proton doping mostly occurs in amorphous PT domains in P3HT films (Inset of Figure 3b) as was the case for F4TCNQ doping in conjugated polymers. PT-C0OH presents even larger shifts in transfer curves. pH response of PT-C0OH films presumably combines contributions of ionic doping effects in PT and proton transfers from carboxylic acid groups (Inset of Figure 3c).

Figure 3d displays  $V_{th}$  distributions of SiO<sub>2</sub>, P3HT, and PT-COOH for different pH solutions over time. 20 consecutive measurements are repeated under each pH solution. pH responses of both P3HT and PT-COOH are mostly reversible, which is opposite to the case of F4TCNQ doping in Figure 2c and shown again here for comparison.  $E_{RG}^{pH}$  and  $E_{RG}^{F4TCNQ}$  of P3HT and PT-COOH are compared in Figure 3e. pH sensitivities of P3HT and PT-COOH are measured to be 18 and 30 mV/pH with a linearity of 80% and 99%, respectively. A difference between  $E_{PT-COOH}^{pH}$  and  $E_{PT}^{pH}$ , which is now designated as  $E_{COOH}^{pH}$ , is 0.098 and 0.158 V for pH 9 and pH 3 solution. To be specific,  $E_{COOH}^{pH}$  is a difference in electrical potential between P3HT and PT-COOH which is affected by concentrations and arrangements of COOH protons. In Figure 3f,  $E_{COOH}^{pH}$  at each pH level ranging from pH3 to 9 is compared with  $E_{COO-}^{ACN}$  that was already calculated in Figure 2c.  $E_{COO-}^{ACN}$  infers less influence of protonation of side chains because it was measured in less polar ACN.  $E_{COOH}^{pH}$  is larger than  $E_{COO-}^{ACN}$  in acidic solutions, meaning COOH in acidic solutions is dominant over COO-. The opposite trend is observed in basic solutions.

Ionic doping effects in doped polymers. Responses of  $E_{PT}^{pH}$  and  $E_{PT-COOH}^{pH}$  for proton concentrations are shown in Figure 4a and 4b, respectively, while P3HT and PT-COOH are sequentially doped by F4TCNQ from 10  $\mu$ g/ml to 1 mg/ml before pH testing.  $E_{PT}^{F4TCNQ}$  and  $E_{PT(+)COO-}^{F4TCNQ}$  are also compared on the right of each plot. Doped P3HT films reveal lower  $E_{pT}^{pH}$  with the increased doping concentartions even in aqueous solutions (Figure 4a). This is because higher work functions of doped films achieved by F4TCNO doping are still maintained. At the same time, proton sensitivity shown in pure P3HT is completely suppressed in the doped P3HT films (Figure 4a and 4c). That is, proton doping mostly occurs in amorphous regions of P3HT films where F4TCNQ anions are already present as counterions for doped P3HT films (Inset of Figure 4a), which corresponds to recent work in the Salleo group that most ionic doping effects occur in amorphous regions of P3HT.33 In contrast, PT-COOH films reveal enhanced pH sensitivities with increasing F4TCNQ doping (Figure 4b, 4c). It could be interpreted that stable carboxylic acid groups which are free to respond to protons are formed in doped PT-COOH due to negative charges on F4TCNQ instead of on carboxylate (Inset of Figure 4b).

We verify our hypothesis above by observing dependency of dopant strength on pH sensitivity of doped polymers. TCNE (Inset of Figure 4d) is a weaker electron acceptor than F4TCNQ. Changes in electric potentials resulting from TCNE doping ( $E_{PT}^{TCNE}$ ) are much smaller than that of  $E_{PT}^{F4TCNQ}$  for the same dopant concentration of 1 mg/ml applied on P3HT (Figure 4d). The same propensity is shown in PT-COOH.

There is no proton response for P3HT:TCNE, as was the case for P3HT:F4TCNQ (Figure 4e, 4f). This shows TCNE fully occupies amorphous domains of P3HT, preventing ionic doping for P3HT:TCNE films. pH sensitivity of PT-COOH:TCNE is largely reduced compared to that of F4TCNQ:PTCOOH (Figure 4e, 4f). This indicates that a weaker electron acceptor TCNE does not inhibit interactions between PT and COOH (Inset of Figure 4f) that would have been evidenced by increased activity of carboxylic acidic groups in aqueous solutions; if anything, the pH responsiveness of PT-COOH was decreased by TCNE.

#### Conclusion

We discovered a facile way to modulate ionic doping effects in CPs using solution sequential molecular doping. The intrinsic pH sensitivity of P3HT of 18 mV/pH is completely eliminated in P3HT:F4TCNQ. It is evident that proton doping mostly occurs in the amorphous domains in P3HT. However, acid-functionalized polythiophene, or PT-COOH, actually shows enhanced pH sensitivity after F4TCNQ doping (40 mV/pH), compared to that of the pure PT-COOH (30 mV/pH). This is because stronger F4TCNQ interactions with the main chain PT-COOH decrease the ionic interactions between PT backbones and COO- side chains, increasing the relative stability of COOH sites in aqueous solutions.

We also verified characteristics of the pure PT-COOH in OECT devices (Figure S10). The OECT shows promising electrical performance with on/off ratio over  $10^3$  and oncurrent level of ca.10 mA for the gate voltage of -0.6 V. Furthermore, the OECT changes threshold voltages depending on pH changes in its solution gate. Sequentially doped PT-COOH:F4TCNQ has promising advantages such as high conductivity, smooth morphology, high stability in aqueous solutions, and functionality for bioconjugations as an alternative to PEDOT:PSS. Furthermore, we expect that suppression of ionic doping effects in PT-COOR:F4TCNQ, where R is a biofunctional group, could offer high specificity for targeting biomarkers under physiological conditions.

## **Experimental Section**

A standard RCA cleaning process was applied for the same sized SiO<sub>2</sub>/Si substrates with 300 nm thickness of oxide. P3HT was synthesized by the following protocol. To a 100 mL, 3-neck round bottom flask, charged with a stir bar, was added 12 mL of anhydrous THF and 2,5-dibromo-3-hexylthiophene (1 g, 3.07 mmol, 1 eq.). A 25 mL dropwise addition funnel was attached where lithium chloride (130 mg, 3.07 mmol, 1 eq) dissolved in 6 mL of anhydrous THF was added. In addition, a solid addition funnel containing Dichloro(1,3-bis(diphenylphosphino)propane) nickel (50 mg, 0.092 mmol, 0.03 eq.) was attached. The vessel was cycled multiple times under vacuum and filled with Argon. After 30 minutes of continuous cycling, the vessel was refilled with Argon. The reaction vessel was then placed on an ice bath and 2.0 M of isopropylmagnesium chloride solution in THF (1.5 mL, 3.07 mmol,1 eq.) was added to the dropwise addition funnel with the dissolved lithium chloride. After 5 minutes of allowing the vessel to stir at 0°C, the iPr-MgCl/LiCl complex was added slowly at dropwise addition. After completion, the reaction vessel was stirred at 0°C for 30 minutes before the ice bath was removed and replaced

with an oil bath with a set temperature of 60°C. The reaction was left to stir for 2 hours before the solid addition funnel was turned and the catalyst was added to the reaction. The solution immediately turned dark red. The reaction was left to stir at 60°C overnight, after which the mixture was precipitated into a well-stirred solution of H<sub>2</sub>O (500 mL) and stirred for 10 min. The resulting suspension was filtered, dried in the oven overnight, and then Soxhlet extracted with hexane, acetone, methanol, and then chloroform in that order. The NMR spectrum of P3HT is shown in Figure S11. Solutions containing a concentration of 20 mg/ml of the synthesized P3HT and PT-COOH purchased from RIEKE (Catalog #:4030) were prepared by dissolving each polymer in chlorobenzene and dimethylformamide, respectively. The prepared solutions were then sonicated for 1 hour and then heated at 60 °C overnight for fully dissolve the polymer while the PT-COOH required the temperature to be raised to 115°C for 20 minutes. P3HT and PT-COOH were then spin coated on SiO<sub>2</sub>/Si under 1600 RPM for 1 min and 1600 RPM for 5 min, respectively. P3HT/SiO<sub>2</sub> and PT-COOH/SiO2 RG were baked at 80 °C for 2 hours. All solutions were filtered using a hydrophobic PTFE or hydrophilic PTFE syringe filter before spincoating. The P3HT and PT-COOH film had a thickness of 46 and 20 nm measured using the Thin Film Analyzer (F20-NIR). A commercial FET (CD4007UB) was used as a transducer to investigate fabricated RGs above. Aqueous solution at defined pH or ACN was placed on each RG surface. A 1 mg/mL solution of F4TCNO (Ossila, 29261-33-4) and TCNE (Sigma Aldrich. 670-54-2) were prepared by dissolving the dopant in ACN aided by ultrasonication for 30 minutes, filtered using a hydrophobic PTFE syringe filter membrane, and then a series dilution was conducted in order to create the range of solution concentrations from 1 mg/ml to 100 ng/ml. 25 µl of each varying concentration of dopant dissolved in acetonitrile was placed on the P3HT surface of the RG module and a Ag/AgCl reference electrode was placed in the solution in order to apply the gate bias for all measurements. All transfer curves were measured by using an Agilent (Keysight) B1500A semiconductor analyzer with a drain voltage set at 50 mV and the gate voltage left at double sweep mode. pH sensitivity of each RG surface was evaluated by using standard pH buffer solution.  $V_{th}$  is calculated as the gate voltage corresponding to drain current of 1  $\mu A$  in each transfer curve. For optical measurements, P3HT and PT-COOH were spin-coated onto Si/SiO<sub>2</sub> (300 nm) substrates that were diced to 1" by 1" dimensions. Confocal laser scanning microscopy (CLSM) and optical microscopic images were collected using a Keyence 3D Laser Scanning Microscope VK-X100/X200 Series that was operated in optical or confocal mode.

## ASSOCIATED CONTENT

**Supporting Information.** Gate current of RGFETs, impedance of a Si-FET and RG structures, OFETs with P3HT and PT-C00H semiconductor, transconductance of RGFETs, Response of SiO<sub>2</sub> surface for F4TCNQ, V<sub>th</sub> distribution of P3HT and PT-C00H as function of F4TCNQ concentrations, and pH sensitivity of SiO<sub>2</sub>. This material is available free of charge via the Internet at http://pubs.acs.org."

## **AUTHOR INFORMATION**

## Corresponding Author

\* hekatz@jhu.edu

#### Present Addresses

†Pritzker School of Molecular Engineering, The University of Chicago, 5640 South Ellis Avenue Chicago, Illinois, USA, 60637

#### **Author Contributions**

Electrical measurements and device fabrication were carried out by H.-J. Jang, Y, Song., and J. Wagner. The manuscript was prepared by H.-J. Jang and H. E. Katz. All authors examined and commented on the manuscript. The project was guided by H. E. Katz.

## **Funding Sources**

The study of P3HT doping was supported by the National Science Foundation, Division of Chemistry, Grant number 1708245. The study of PT-COOH doping and pH response was supported by the National Science Foundation, Division of Materials Research, Grant number 1807292.

#### Notes

Any additional relevant notes should be placed here.

## **ACKNOWLEDGMENT**

The study of P3HT doping was supported by the National Science Foundation, Division of Chemistry, Grant number 1708245. The study of PT-COOH doping and pH response was supported by the National Science Foundation, Division of Materials Research, Grant number 1807292.

## **REFERENCES**

- (1) Song, J.; Dailey, J.; Li, H.; Jang, H. J.; Zhang, P. F.; Wang, J. T. H.; Everett, A. D.; Katz, H. E. Extended Solution Gate OFET-Based Biosensor for Label-Free Glial Fibrillary Acidic Protein Detection with Polyethylene Glycol-Containing Bioreceptor Layer. *Adv. Funct. Mater.* **2017**, *27* (20)
- (2) Khan, H. U.; Roberts, M. E.; Johnson, O.; Forch, R.; Knoll, W.; Bao, Z. N. In Situ, Label-Free DNA Detection Using Organic Transistor Sensors. *Adv Mater* **2010**, *22* (40), 4452-4456.
- (3) Jang, H. J.; Ahn, J.; Kim, M. G.; Shin, Y. B.; Jeun, M.; Cho, W. J.; Lee, K. H. Electrical Signaling of Enzyme-Linked Immunosorbent Assays with an Ion-Sensitive Field-Effect Transistor. *Biosens. Bioelectron.* **2015**, *64*, 318-323.
- (4) Seo, G.; Lee, G.; Kim, M. J.; Baek, S. H.; Choi, M.; Ku, K. B.; Lee, C. S.; Jun, S.; Park, D.; Kim, H. G.; Kim, S. J.; Lee, J. O.; Kim, B. T.; Park, E. C.; Kim, S. I. Rapid Detection of COVID-19 Causative Virus (SARS-CoV-2) in Human Nasopharyngeal Swab Specimens Using Field-Effect Transistor-Based Biosensor. *ACS Nano* **2020**, *14* (4), 5135-5142.
- (5) Trung, T. Q.; Ramasundaram, S.; Hwang, B. U.; Lee, N. E. An All-Elastomeric Transparent and Stretchable Temperature Sensor for Body-Attachable Wearable Electronics. *Adv. Mater.* **2016**, *28* (3), 502-509.
- (6) Gualandi, I.; Tonelli, D.; Mariani, F.; Scavetta, E.; Marzocchi, M.; Fraboni, B. Selective Detection of Dopamine with an All PEDOT:PSS Organic Electrochemical Transistor. *Sci. Rep.* **2016**, *6*, 35419.
- (7) Gualandi, I.; Marzocchi, M.; Scavetta, E.; Calienni, M.; Bonfiglio, A.; Fraboni, B. A Simple All-PEDOT: PSS Electrochemical Transistor for Ascorbic Acid Sensing. *J. Mater. Chem. B* **2015**, *3* (33), 6753-6762.

- (8) Gkoupidenis, P.; Schaefer, N.; Garlan, B.; Malliaras, G. G. Neuromorphic Functions in PEDOT:PSS Organic Electrochemical Transistors. *Adv. Mater.* **2015**, *27* (44), 7176-80.
- (9) Lu, W.; Fadeev, A. G.; Qi, B. H.; Smela, E.; Mattes, B. R.; Ding, J.; Spinks, G. M.; Mazurkiewicz, J.; Zhou, D. Z.; Wallace, G. G.; MacFarlane, D. R.; Forsyth, S. A.; Forsyth, M. Use of Ionic Liquids for Pi-Conjugated Polymer Electrochemical Devices. *Science* **2002**, *297* (5583), 983-987.
- (10) Fan, X.; Nie, W. Y.; Tsai, S. H.; Wang, N. X.; Huang, H. H.; Cheng, Y. J.; Wen, R. J.; Ma, L. J.; Yan, F.; Xia, Y. G. PEDOT:PSS for Flexible and Stretchable Electronics: Modifications, Strategies, and Applications. *Adv. Sci.* **2019**, *6* (19).
- (11) Kim, S. M.; Kim, C. H.; Kim, Y.; Kim, N.; Lee, W. J.; Lee, E. H.; Kim, D.; Park, S.; Lee, K.; Rivnay, J.; Yoon, M. H. Influence of PEDOT:PSS Crystallinity and Composition on Electrochemical Transistor Performance and Long-Term Stability. *Nat. Commun.* **2018**, *9*.
- (12) Parlak, O.; Keene, S. T.; Marais, A.; Curto, V. F.; Salleo, A. Molecularly Selective Nanoporous Membrane-based Wearable Organic Electrochemical Device for Noninvasive Cortisol Sensing. *Sci. Adv.* **2018**, *4* (7), eaar2904.
- (13) Nielsen, C. B.; Giovannitti, A.; Sbircea, D. T.; Bandiello, E.; Niazi, M. R.; Hanifi, D. A.; Sessolo, M.; Amassian, A.; Malliaras, G. G.; Rivnay, J.; McCulloch, I. Molecular Design of Semiconducting Polymers for High-Performance Organic Electrochemical Transistors. *J. Am. Chem. Soc.* **2016**, *138* (32), 10252-10259.
- (14) Strakosas, X.; Sessolo, M.; Hama, A.; Rivnay, J.; Stavrinidou, E.; Malliaras, G. G.; Owens, R. M. A Facile Biofunctionalisation Route for Solution Processable Conducting Polymer Devices. *J. Mater. Chem. B* **2014**, *2* (17), 2537-2545.
- (15) Gentili, D.; D'Angelo, P.; Militano, F.; Mazzei, R.; Poerio, T.; Brucale, M.; Tarasbella, G.; Bonetti, S.; Marasso, S. L.; Cocuzza, M.; Giorno, L.; Iannotta, S.; Cavallini, M. Integration of Organic Electrochemical Transistors and Immuno-Affinity Membranes for Label-free Detection of Interleukin-6 in the Physiological Concentration Range through Antibody-Antigen Recognition. *J. Mater. Chem. B* **2018**, *6* (33), 5400-5406,
- (16) Macchia, E.; Manoli, K.; Holzer, B.; Di Franco, C.; Ghittorelli, M.; Torricelli, F.; Alberga, D.; Mangiatordi, G. F.; Palazzo, G.; Scamarcio, G.; Torsi, L. Single-molecule Detection with a Millimetre-Sized Transistor. *Nat. Commun.* **2018**, *9*, 3223.
- (17) Wang, N. X.; Yang, A. N.; Fu, Y.; Li, Y. Z.; Yan, F. Functionalized Organic Thin Film Transistors for Biosensing. *Acc. Chem. Res.* **2019**, *52* (2), 277-287.
- (18) Savva, A.; Cendra, C.; Giugni, A.; Torre, B.; Surgailis, J.; Ohayon, D.; Giovannitti, A.; McCulloch, I.; Di Fabrizio, E.; Salleo, A.; Rivnay, J.; Inal, S. Influence of Water on the Performance of Organic Electrochemical Transistors. *Chem. Mater.* **2019**, *31*, 927.
- (19) Jacobs, I. E.; Aasen, E. W.; Oliveira, J. L.; Fonseca, T. N.; Roehling, J. D.; Li, J.; Zhang, G. W.; Augustine, M. P.; Mascal, M.; Moule, A. J. Comparison of Solution-mixed and Sequentially Processed P3HT:F4TCNQ Films: Effect of Doping-induced Aggregation on Film Morphology. *J. Mater. Chem. C* **2016**, *4* (16), 3454-3466.
- (20) Mai, C. K.; Schlitz, R. A.; Su, G. M.; Spitzer, D.; Wang, X. J.; Fronk, S. L.; Cahill, D. G.; Chabinyc, M. L.; Bazan, G. C. Side-Chain Effects on the Conductivity, Morphology, and Thermoelectric Properties of Self-Doped Narrow-Band-Gap Conjugated Polyelectrolytes. *J. Am. Chem. Soc.* **2014**, *136* (39), 13478-13481.
- (21) A. O. PATIL, Y. I., N. BASESCU, N. COLANERI, J. CHEN, F. WUDL and A. J. HEEGER. Self-Doped Conducting Polymers. *Synth. Met.* **1987**, *20*, 151 159.
- (22) Mervin Chun-Yi Ang, C. G. T., Qi-Mian Koh, Chao Zhao, Qiu-Jing Seah, Yu Wang, Martin Callsen, Yuan-Ping Feng, Rui-Qi Png and Lay-Lay Chu. Bulk Ion-clustering and Surface Ion-Layering Effects on Work Function of Self-compensated Charged-doped Polymer Semiconductors. *Mater. Horiz.* **2020**, *7*, 1073-1082.
- (23) Jang, H. J.; Wagner, J.; Li, H.; Zhang, Q.; Mukhopadhyaya, T.; Katz, H. E. Analytical Platform To Characterize Dopant Solution Concentrations, Charge Carrier Densities in Films and Interfaces,

- and Physical Diffusion in Polymers Utilizing Remote Field-Effect Transistors. *J. Am. Chem. Soc.* **2019**, *141* (12), 4861-4869.
- (24) Chew, A. R.; Ghosh, R.; Shang, Z. R.; Spano, F. C.; Salleo, A. Sequential Doping Reveals the Importance of Amorphous Chain Rigidity in Charge Transport of Semi-Crystalline Polymers. *J. Phys. Chem. Lett.* **2017**, *8* (20), 4974-4980.
- (25) Scholes, D. T.; Hawks, S. A.; Yee, P. Y.; Wu, H.; Lindemuth, J. R.; Tolbert, S. H.; Schwartz, B. J. Overcoming Film Quality Issues for Conjugated Polymers Doped with F4TCNQ by Solution Sequential Processing: Hall Effect, Structural, and Optical Measurements. *J. Phys. Chem. Lett.* **2015**, *6* (23), 4786-93.
- (26) Scholes, D. T.; Yee, P. Y.; Lindemuth, J. R.; Kang, H.; Onorato, J.; Ghosh, R.; Luscombe, C. K.; Spano, F. C.; Tolbert, S. H.; Schwartz, B. J. The Effects of Crystallinity on Charge Transport and the Structure of Sequentially Processed F(4)TCNQ-Doped Conjugated Polymer Films. *Adv. Funct. Mater.* **2017**, *27*, 1702654.
- (27) Duong, D. T.; Phan, H.; Hanifi, D.; Jo, P. S.; Nguyen, T. Q.; Salleo, A. Direct Observation of Doping Sites in Temperature-Controlled, p-Doped P3HT Thin Films by Conducting Atomic Force Microscopy. *Adv. Mater.* **2014**, *26*, 6069.
- (28) Gao, J.; Roehling, J. D.; Li, Y.; Guo, H.; Moule, A. J.; Grey, J. K. The Effect of 2,3,5,6-tetrafluoro-7,7,8,8-tetracyanoquinodimethane Charge Transfer Dopants on the Conformation and Aggregation of Poly(3-hexylthiophene). *J. Mater. Chem. C* 2013, 1 (36), 5638-5646. (29) Gao, J.; Niles, E. T.; Grey, J. K. Aggregates Promote Efficient Charge Transfer Doping of Poly(3-hexylthiophene). *J. Phys. Chem. Lett.* 2013, 4 (17), 2953-2957.
- (30) Justine Wagner, H.-J. J., Jinfeng Han and Howard E. Katz. Enhanced and unconventional responses in chemiresistive sensing devices for nitrogen dioxide and ammonia from carboxylated alkylthiophene polymers. *Mater. Horiz.* **2020**, *7*, 1358.
- (31) Pullano, S. A.; Critello, C. D.; Mahbub, I.; Tasneem, N. T.; Shamsir, S.; Islam, S. K.; Greco, M.; Fiorillo, A. S. EGFET-Based Sensors for Bioanalytical Applications: A Review. *Sensors* **2018**, *18*. 4042
- (32) David E. Yates, S. L., Thomas W. Healy. Site-Binding Model of the Electrical Double Layer at the OxideWater Interface. *J. Chem. Soc., Faraday Trans.* 1, **1973**, *70*, 1807-1818.
- (33) Guardado, J. O.; Salleo, A. Structural Effects of Gating Poly(3-hexylthiophene) through an Ionic Liquid. *Adv. Funct. Mater.* **2017**, *27*, 1701791.

## **Table of Contents**

